Nonequilibrium phenomena in N_2-cluster–surface collisions: A molecular-dynamics study of fragmentation, lateral jetting, and nonequilibrium energy distributions

Steffen Zimmermann and Herbert M. Urbassek*
Fachbereich Physik, Universität Kaiserslautern, Erwin-Schrödinger-Straße, D-67663 Kaiserslautern, Germany
(Received 20 September 2006; published 14 December 2006)

Using molecular-dynamics simulation, we study the impact of $(N_2)_{2869}$ clusters on a flat rigid wall. We study the cluster fragmentation process, the formation of lateral jets, the energy redistribution among the resulting fragments, and the ratio of internal and translational energy of the emerging free molecules as a function of cluster impact energy in the range of 0.076–1520 meV/molecule. We find the fragmentation threshold energy to be in agreement with that found previously for $(N_2)_{13}$ clusters; the (scaled) number of fragments, however, increases more slowly with impact energy. Also the energy redistribution of the cluster impact energy among the internal and translational energy of the fragments is similar to that found for the small cluster. This means in particular that free molecules show a strong nonequilibrium energy partitioning in which the internal degrees of freedom are considerably less excited than the translational degrees of freedom. We also find that at impact energies above the fragmentation threshold the angular distribution of fragments is peaked parallel to the surface—i.e., the formation of lateral surface jets.

DOI: 10.1103/PhysRevA.74.063203 PACS number(s): 36.40.−c, 68.49.Fg, 79.20.Ap

I. INTRODUCTION

The cluster-surface interaction is a phenomenon which is receiving increased attention due to its importance in many fields of science. From an applied point of view, controlled cluster deposition [1] (soft landing) [2] or surface cleaning by cluster impact [3] give promising prospects. In the field of cluster-impact chemistry [4], a number of intriguing experiments on cluster fragmentation, collisional energy loss, collision-induced dissociation, and even impact-induced chemical reactions have been performed and accompanied by molecular-dynamics simulations. From a fundamental point of view, processes such as short-time extreme local densities, pressures, and kinetic temperatures reached [5] or induced electronic excitations [6] were investigated.

Simulational studies of cluster-surface interactions have been performed on several levels of sophistication. On the one hand, fluid-dynamical simulations have been presented. As an example, we mention the study by Haller *et al.* [7] of a high-speed (500 m/s), 0.2-mm-sized liquid droplet with parameters pertaining to water colliding against a rigid wall. This investigation as well as previous studies, [8], demonstrates the phenomenon of "splashing" or "lateral jetting," in which the droplet spreads out with high speed radially along the surface of the wall. Another approach uses atomistic simulation, in particular molecular-dynamics simulation, to describe the phenomena occurring during and after cluster-surface interaction [9–11]. In these studies, the cluster size has to be taken considerably smaller, less than a few tens of nanometers, say. On the other hand, molecular-dynamics simulations allow one to include in a natural way atomistic phenomena such as cluster fragmentation, internal excitation, the influence of internal degrees of freedom, etc.

Thus, molecular-dynamics simulations [5,11–16] of the impact of rare-gas clusters on surfaces have demonstrated the extensive or even complete fragmentation of the impinging cluster occurring at higher impact velocities. Also, simulations of specific molecular clusters such as $(NH_3)_nH^+$ and also of mixed species such as I_2Ar_n and $(CH_3I)_n^-$ have been performed [16–18]. In these studies, as a rule only the rotational degrees of freedom of the molecules were included. In another interesting study [11], Christen *et al.* showed in a combined experimental and simulational approach that at low cluster velocities a regime of "deep inelastic scattering" occurs where the clusters lose most of their initial kinetic energy upon scattering off the surface. In earlier papers [15,19], Raz *et al.* used a maximum-entropy argument to show that the transition from (low-energy) evaporation of a few atoms to (high-energy) shattering into many fragments shows a rather sharp transition as a function of the impact energy. This transition was termed the "shattering transition" and occurs when the cluster energy per atom exceeds the bond energy, or in other words, the cluster temperature exceeds the "boiling temperature."

In a recent study [20], the phenomena occurring after $(N_2)_{13}$ impact on a rigid wall were described in detail and the various fragmentation regimes (intact reflection, partial and complete fragmentation) could be discussed. By comparing the impact of the molecular cluster with an equal-mass atomic cluster, the influence of the internal molecular degrees of freedom could be demonstrated; these lead to a reduction of the translational energy of the fragments and the nonequilibrium nature of the redistribution of the cluster energy among the different degrees of freedom.

In the present paper we present results for the reflection of a larger N_2 cluster consisting of 2869 molecules from a rigid wall. This will allow us to discuss the influence of cluster size on the reflection behavior for an exemplary case. While a systematic study of the effect of cluster size on the cluster-surface scattering dynamics is certainly interesting, we follow here the strategy of supplementing our previous study [20] on small clusters with one representative investigation for one larger cluster size; this allows us to identify by way

*Electronic address: urbassek@rhrk.uni-kl.de; URL: http://www.physik.uni-kl.de/urbassek/

of example those issues where cluster size plays an important role from those where it is of subordinate importance. We furthermore concentrate on scattering off a purely repulsive surface, since our recent study [20] showed that the inclusion of an attractive well—which is certainly both of fundamental interest and of practical importance—strongly complicates the analysis of the collision process. It will turn out that many features of the fragmentation, behavior, and in particular the onset of fragmentation are quite similar for small and large clusters. One might have assumed that with increasing cluster size, the distribution of emitted molecular fragments will be closer to an equilibrium thermal distribution. We will present evidence that—at least for the cluster size investigated—this is not true and the various degrees of freedom of the ensemble of molecular fragments are not in equilibrium. However, our results show the phenomenon of lateral jetting, which has not been seen for the small-cluster impact, but is so evident both in experiment and in fluid-dynamic simulations of larger-cluster impacts [7,8].

II. SYSTEM

A. Cluster

We study the reflection of an icosahedral cluster, containing $n=2869$ N_2 molecules, from a rigid wall. The cluster has been constructed as a so-called Mackay icosahedron [21–23]. While it could be shown only for smaller clusters, containing $\lesssim 150$ atoms, that this structure provides the global minimum of the potential energy for Lennard-Jones, and also Au, atomic clusters [24,25], we assume that the icosahedral structure provides a convenient low-lying minimum configuration for simulating the collision event. The results are compared to the reflection of an $(N_2)_{13}$ cluster [20], which is also of an icosahedral shape.

The intramolecular bonding has been chosen as a Morse potential

$$V_{\text{intra}}(r) = D[e^{-2(r-r_0)/\lambda} - 2e^{-(r-r_0)/\lambda}], \tag{1}$$

with parameters $D=9.99$ eV, $r_0=1.0977$ Å, and $\lambda=0.2696$ Å; [26,27]; the mass of an N atom is $m=14$ amu. The intermolecular interaction potential, acting between atoms belonging to different molecules only, is chosen as an atomic pairwise Lennard-Jones potential

$$V_{\text{inter}}(r) = 4\epsilon\left[\left(\frac{\sigma}{r}\right)^{12} - \left(\frac{\sigma}{r}\right)^{6}\right], \tag{2}$$

with parameters $\epsilon=3.212$ meV and $\sigma=3.31$ Å [28,29]. The total intermolecular binding energy of the cold cluster will be denoted by Φ and amounts to

$$\Phi = 194.122 \text{ eV}. \tag{3}$$

B. Wall

The rigid, uncorrugated wall considered in this study is modeled by an external potential, which acts on each cluster atom and depends only on the perpendicular distance z of the atom to the wall. We adopt a purely repulsive potential

$$V_{\text{wall}}^{\text{rep}}(z) = \begin{cases} 4\epsilon_w\left[\left(\frac{\sigma_w}{z}\right)^{12} - \left(\frac{\sigma_w}{z}\right)^{6}\right] + \epsilon_w, & z < 2^{1/6}\sigma_w, \\ 0, & z \geq 2^{1/6}\sigma_w. \end{cases} \tag{4}$$

The potential parameters ϵ_w and σ_w are chosen to have the same values as for the intermolecular interaction of the N_2 molecules, Eq. (2).

C. Simulation

The molecular-dynamics code is standard [30]. It employs the velocity Verlet integrator to solve Newton's equations of motion. In order to resolve the vibrational motion in the molecular systems, the time step is chosen rather small, 0.1 fs.

In the simulation, the cluster is initially positioned at a distance $z>2^{1/6}\sigma_w$ in front of the wall such that the cluster has no interaction with it. The cluster is at temperature zero; it does not vibrate or rotate. Each simulation has been performed with two cluster orientations: (i) with a molecule pointing towards the surface (tip geometry) and (ii) with a cluster face pointing towards the surface (face geometry). Since the differences in the results of these two orientations are only minor, in the following only the averages over these two orientations will be discussed.

The cluster is given a kinetic center-of-mass energy nE_0 with a momentum directed perpendicular to the surface. We study energies E_0 ranging from 0.076 to 1520 meV/molecule; the corresponding center-of-mass velocities of the clusters are between 23 m/s and 3.3 km/s. The simulation proceeds until 100 ps, when the cluster has been totally reflected from the surface—i.e., until all cluster atoms are again outside the interaction potential of the wall.

III. RESULTS

A. Overview

In Fig. 1 we present side views of the cluster-surface impact event. In all cases, we see that the cluster strongly flattens during the impact and assumes at around 25 ps a disklike shape upon the surface. During this time it has been heated up, and for all impact energies, at least a few free molecules have been emitted from it. For the lowest impact energy, 38 meV/molecule, the cluster recovers its spherical shape after 100 ps; it has lost almost all its translational energy due to the inelasticity of the collision. For the higher energies shown the cluster breaks up into several large clusters which move radially outward.

Note that at the earliest time displayed, at 5 ps, the bottom of the cluster has been strongly heated. The top side is still intact for the lowest impact energy while the shock front emitted from the impact has already come close to the top for the highest impact energy; similar phenomena have been seen in the fluid-dynamical study of Haller *et al.* [7]. The structure displayed at 10 ps is interesting in that the maximum height of the cluster is not reached above the cluster center; rather, a crater has been formed there surrounded by a ringlike rim. This feature does not seem to have been observed in fluid simulations. We presume that it has the fol-

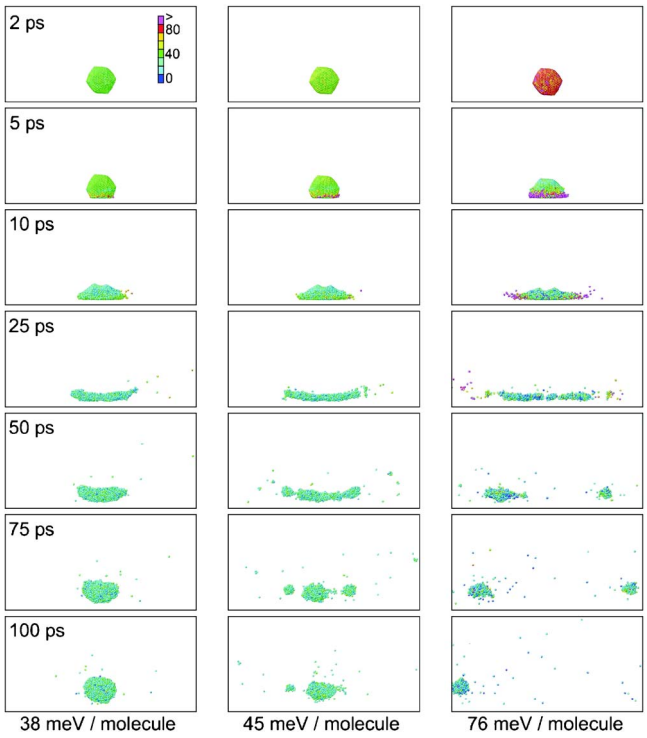

FIG. 1. (Color online) Time series of events after impact of a $(N_2)_{2869}$ cluster on a surface. Molecules are colored according to their kinetic energy, measured in meV/molecule. This side view displays only molecules in a slab of thickness 60 Å in viewing direction. The figure extends laterally to a size of 350 Å.

lowing origin: When the cluster tip reaches the surface, a high pressure develops immediately below the cluster center. Due to the high compressibility of the N_2 cluster, it is compressed here most. When finally the sides of the cluster also contact the surface, the pressure developing there can be relieved by a lateral flow and hence the hatlike structure of Fig. 1 at 10 ps results.

Figure 2 shows top views at two selected moments of time, $t=25$ and $t=100$ ps, of the impacts displayed in Fig. 1. At $t=25$ ps, the onset of radial emission of fragments along the surface is clearly seen for the highest impact energy; this cluster finally fragments into several larger clusters and a cloud of free molecules. At the smallest impact energy, the spherical cluster shape is recovered, while the middle impact energy shows the fission of the impinging cluster into two asymmetrically sized clusters.

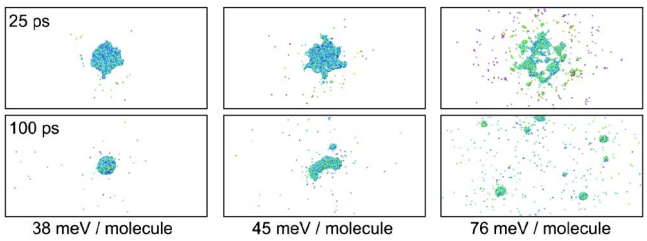

FIG. 2. (Color online) Top view of the events shown in Fig. 1 at the time of $t=25$ and 100 ps.

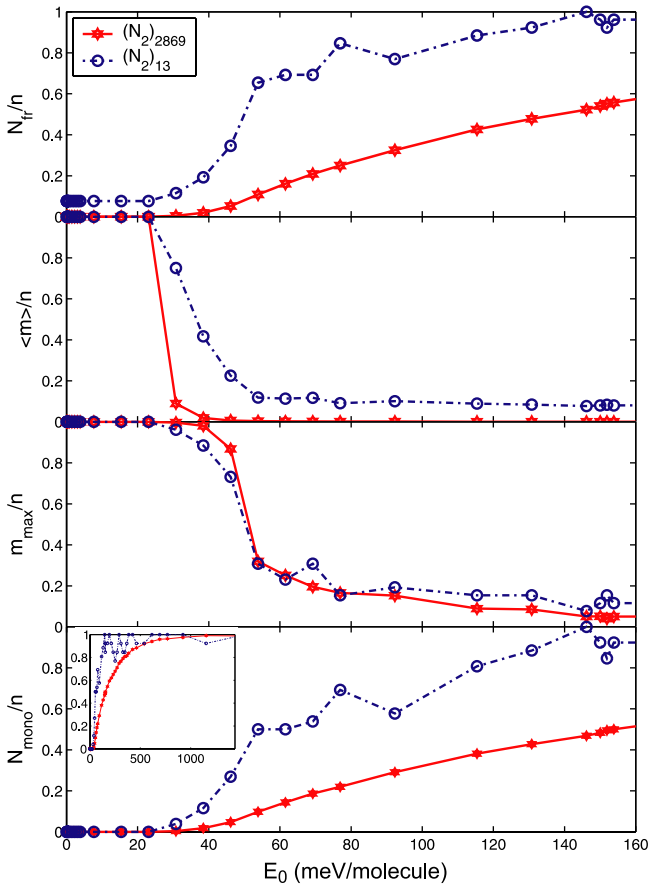

FIG. 3. (Color online) Fragmentation behavior of the cluster after collision with a repulsive wall: (a) average number of fragments, N_{fr}; (b) average fragment size $\langle m \rangle$; (c) size of the largest fragment, m_{max}; (d) average number of free molecules, N_{mono}. In order to show the results for both the $(N_2)_{2869}$ and $(N_2)_{13}$ clusters in the same plots, the data have been scaled to the total number of molecules, n, initially present in the cluster.

B. Fragmentation

In order to quantify the fragmentation process, we identify the set of fragments at the end of the simulation, 100 ps, using a cluster-detection algorithm [31]. This algorithm subdivides all atoms into disjoint sets; the atoms in any such set have zero interaction energy with the atoms of the other sets, but nonzero interaction with at least one other atom of the same set. We identify these disjoint sets with the cluster fragments produced by the collision with the wall. The fragment distribution is then characterized using several quantities: the number of fragments produced, N_{fr}; the average fragment size $\langle m \rangle$; the size of the largest fragment, m_{max}; and the number of free molecules produced, N_{mono}.

Figure 3 shows these characteristics of the cluster fragmentation process. For comparison, previous results obtained for $(N_2)_{13}$ impact are included. We see that fragmentation sets in at a threshold energy

$$E_{th}^{frag} = 30 \text{ meV/molecule}. \quad (5)$$

This threshold is identical to that found previously for $(N_2)_{13}$ clusters. We believe that this is no accident, but that

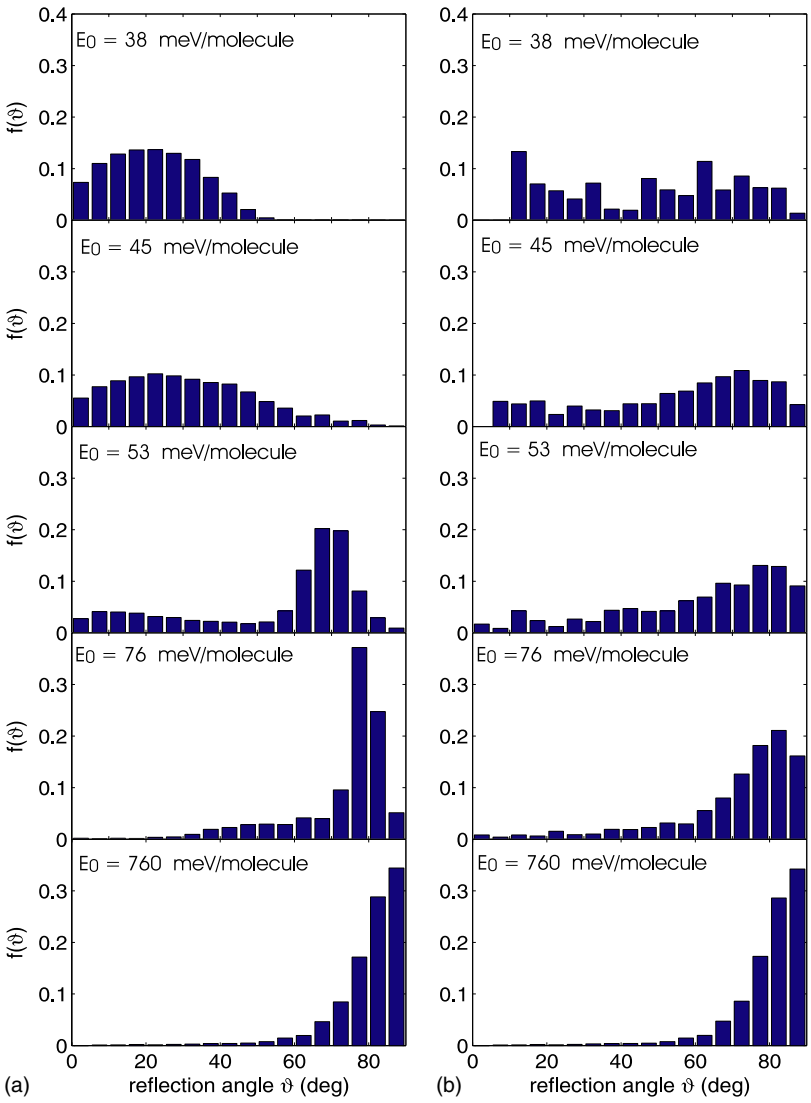

FIG. 4. (Color online) Angular distribution $f(\vartheta)$ after impact of a $(N_2)_{2869}$ cluster on a surface. ϑ is the angle towards the surface normal. Data have been normalized to $\int f(\vartheta)\sin\vartheta d\vartheta = 1$. (a) All molecules. (b) Only free molecules.

the fragmentation threshold is determined by an adiabaticity argument, which only depends on the cluster speed and the intermolecular bond energy [20,32]: Vibrations are not excited, and hence bonds are not broken, if the collision time $t_c = \sigma_w / v$ is larger than the vibration period $T = 2\pi/\omega$. Here $v = \sqrt{E_0/m}$ is the translational velocity of the cluster and $\omega = 12 \times 2^{-1/6}\sqrt{\epsilon/m\sigma^2}$ is the vibrational frequency of the Lennard-Jones potential. Thus impact energies $E_0 > 9.3$ meV/molecule are required to excite intermolecular vibrations. Full breaking of these bonds, of course, needs higher energies, which explains our simulation result for the fragmentation threshold of 30 meV/molecule, Eq. (5).

We note that the scaled fragmentation quantities presented in Fig. 3 show a rather similar energy dependence for the small and large clusters. However, saturation of the fragmentation—i.e., full fragmentation into free molecules—is only reached more slowly and at a higher energy for the large cluster. Thus, we need an impact energy of around 600 meV/molecule until 90% of the N_2 molecules are free for $(N_2)_{2869}$ impact, while this is reached already at roughly 200 meV/molecule for the small cluster—even though this quantity shows larger fluctuations in this case.

C. Angular distribution

We measure the angular distribution $f(\vartheta)$ at time $t = 100$ ps after impact in the following way. For each molecule, we determine the angle ϑ between its center of mass (seen from the base point of the impacting cluster) and the surface normal. $f(\vartheta)\sin\vartheta d\vartheta$ is the number of molecules, emitted in direction $(\vartheta, \vartheta + d\vartheta)$. We normalize the distribution to $\int f(\vartheta)\sin\vartheta d\vartheta = 1$.

Figure 4 displays the angular distributions for several impact energies. Both the angular distribution of *all* molecules [Fig. 4(a)]—irrespective of whether they have been emitted as free molecules or are still bound to a larger cluster fragment—and the distributions of exclusively the free molecules [Fig. 4(b)] are shown. Slightly above the fragmentation threshold ($E_0 = 38$–45 meV/molecule), the angular distribution of free molecules is broadly and more or less uniformly distributed. For these energies, the distribution of all molecules peaks at near-normal angles, with values extending up to a around 40°–60°. This distribution characterizes the "reflected" cluster fragments, while free molecules have been emitted uniformly in all directions. With increas-

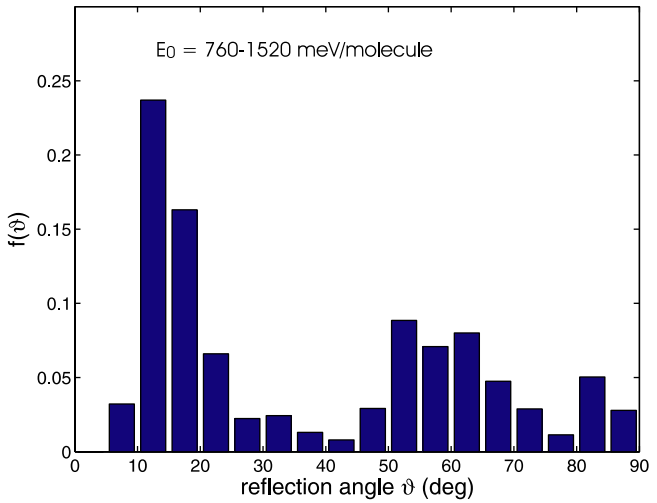

FIG. 5. (Color online) Analogous to Fig. 4, but for a $(N_2)_{13}$ cluster. All molecules are displayed. Data for impact energies E_0 =760–1520 meV/molecule have been included.

ing impact energy, the distribution moves more and more towards the surface plane, until at 380 meV/molecule, it shows a pronounced peak in this plane. This feature holds true both for the free molecules and for the distribution of all molecules.

The emission of particles in the surface plane has been termed *lateral jetting* and has been observed already previously in fluid-dynamic simulations of liquid droplet-surface impact phenomena. Its origin is the inertia of the rear part of the impacting cluster, which moves towards the surface, while the front part is already colliding with the surface; thus, the front atoms are accelerated sideways out of the collision zone and give rise to the observed lateral jets.

Figure 5 shows for comparison the angular emission distribution for $(N_2)_{13}$ clusters. Here, in order to improve the statistics, the distributions of four impact energies in the range of E_0=760–1520 meV/molecule have been added. Clearly, the small cluster shows a broad distribution. A pronounced peak in near-normal "reflection" direction is visible, while the lateral-jet peak ($\vartheta > 85°$) is not observed here.

D. Energy redistribution

After collision with the surface, the total impact energy nE_0 is found again in the ensemble of reflected cluster fragments. For the molecular N_2 clusters no molecular dissociation and (almost) no vibrational excitation occur. Hence, the impact energy can be used only for cluster fragmentation, internal fragment-cluster excitation, rotational excitation of free molecules, and in the translational energy of cluster fragments and free molecules moving away from the surface. Our energy balance reads

$$E_0 = E_{\text{trans}} + E_{\text{int}}^{\text{kin}} + E_{\text{int}}^{\text{pot}} + E_{\text{rot}}. \tag{6}$$

We define these energies as follows: Let us call N_{fr} the number of fragments produced. For each fragment κ, we calculate the center-of-mass energy $E_{\text{c.m.},\kappa}$ and call

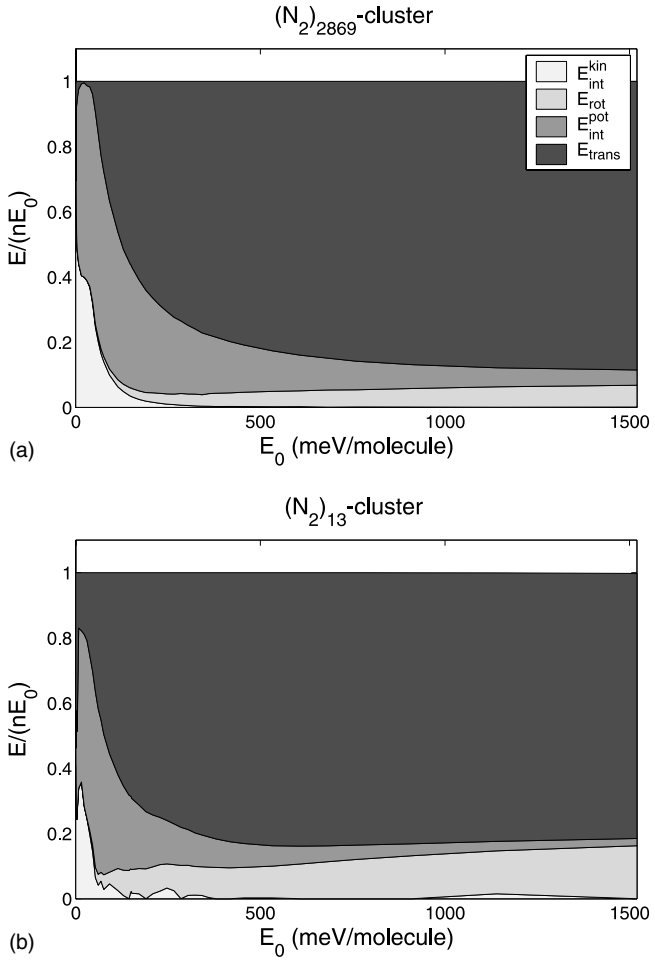

FIG. 6. Energy redistribution in a $(N_2)_{2869}$ (a) and a $(N_2)_{13}$ (b) cluster after reflection from the surface. Energies are displayed relative to impact energy nE_0.

$$E_{\text{trans}} = \sum_{\kappa=1}^{N_{\text{fr}}} E_{\text{c.m.},\kappa} \tag{7}$$

the translational energy. Note that these center-of-mass energies $E_{\text{c.m.},\kappa}$ are observable in experiment by time-of-flight techniques.

In accordance with the potentials, Eqs. (1) and (2), which fulfill $V(r \to \infty) = 0$, all potential energies given below refer to the reference state of a completely fragmented cluster. We shall call

$$E_{\text{int}}^{\text{pot}} = \sum_{i<j} V_{\text{inter}}(r_{ij}) + \Phi \tag{8}$$

the increase in potential energy due to (partial) fragmentation of the parent cluster and internal excitation of the fragments.

The remaining energy is internal kinetic energy of the free molecules and cluster fragments. We introduce E_{rot} as the rotational energy of free molecules and $E_{\text{int}}^{\text{kin}}$ as the internal kinetic energy of cluster fragments.

Figure 6 shows the energy redistribution of the large $(N_2)_{2869}$ and small $(N_2)_{13}$ clusters. The general trends are similar: The fragmentation threshold is characterized by a

maximum internal excitation and a minimum translational energy of the cluster. However, for the larger cluster, the translational energy virtually vanishes at this point; here, the collision of the cluster with the surface is truly entirely inelastic and all the impact energy of the cluster is converted into internal energy. With increasing impact energy, a relatively larger portion is given to the translational energy of the fragments. The kinetic energy of the internal motion, $E_{\mathrm{int}}^{\mathrm{kin}}$, decreases and finally vanishes when no cluster fragments besides free molecules have survived. The potential energy $E_{\mathrm{int}}^{\mathrm{pot}}$ stays constant at this point as it consists of the entire fragmentation energy of the parent cluster; its relative contribution in Fig. 6, however, decreases. Note that the relative contribution of potential energy due to fragmentation, $E_{\mathrm{int}}^{\mathrm{pot}}$, is higher for the large than for the small cluster: This reflects the larger number of bonds available in the $(N_2)_{2869}$ molecule, resulting in an average bond energy of 67.7 meV/molecule as compared to 33.8 meV/molecule for the $(N_2)_{13}$ cluster.

Note that the rotational energy of free molecules fragmented from the large cluster is considerably smaller than those emitted from the small cluster. This feature may be due to the smaller collision time of the $(N_2)_{13}$ parent cluster with the surface and the correspondingly more violent collision event. The larger $(N_2)_{2869}$ cluster spends more time in the collision, since the trailing rear part of the cluster tends to contain the collision zone and hence allows for more intermolecular interaction. As a consequence, rotations are less excited and more energy is given to translation.

The rotational excitation of free molecules carries an increasing portion of the impact energy. This aspect is further analyzed in Fig. 7(a), where the relative contributions of the energy of free molecules, E_{mol}, is displayed. Only the molecules in the lateral jet—i.e., with emission angles $\vartheta > 85°$—are displayed; since these form the majority, their behavior is representative. It is seen that even though rotational excitation is strong, it carries only a small fraction of the total energy E_{mol}, amounting to a fraction of only around 4%–7% of the translation energy. This fraction is quite constant for impact energies above around 100 meV/molecule. The ratio between rotational and translational energies is far away from that holding in thermodynamic equilibrium which is governed by the activated degrees of freedom and would be 2/3; this gives evidence of the strongly nonequilibrium nature of the monomer formation process.

Figure 7(b) quantifies how many molecules out of the $n=2869$ of the impinging cluster are emitted parallel to the surface—i.e., with an angle of $\vartheta > 85°$—and thus contribute to the lateral jets. It is seen that above the fragmentation threshold, this portion steadily increases and reaches a maximum at around 400 meV/molecule; at this energy, the contribution of cluster fragments in the flow of reflected particles becomes negligible. For higher impact energies, the fraction of molecules in the lateral jet slightly decreases again, since for decreasing collision times, the inertia of the rear part of the cluster, which is responsible for the lateral-jet formation, will have less time to influence the fragment flow.

E. Model study of vibrational excitation

N_2 molecules are not vibrationally excited at the impact energies considered here. This is due to the stiffness of the

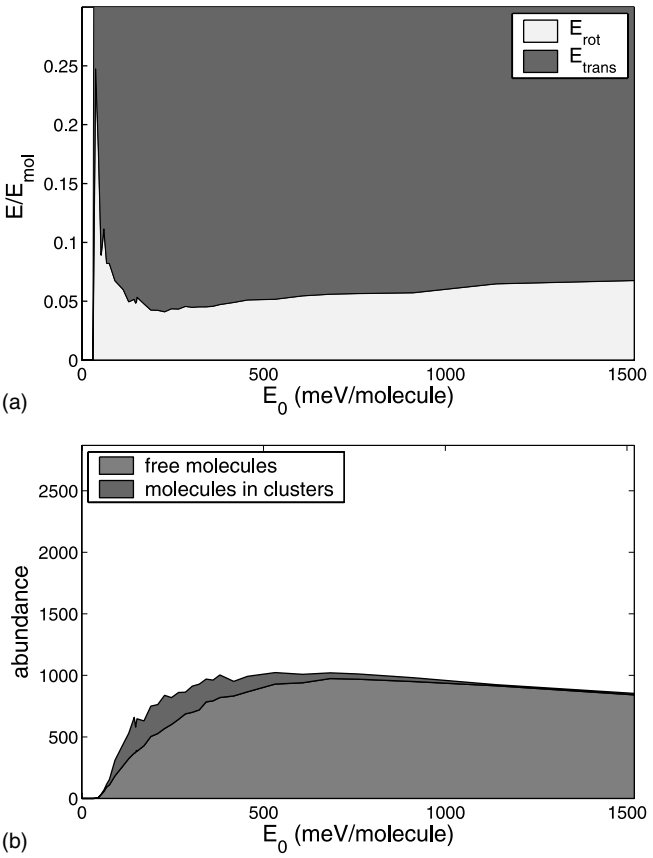

FIG. 7. Characteristics of free molecules emitted into the lateral jets ($\vartheta > 85°$). (a) Partitioning of the energy E_{mol} of free N_2 molecules emerging from $(N_2)_{2869}$-surface collisions into their rotational and translational contributions. (b) Number of molecules bound in clusters and free molecules emitted parallel to the surface.

N_2 intramolecular bond. In order to investigate the role of vibrational excitation we performed simulations for a model molecule, which we call ψ_2. All its properties are identical to N_2; only the intramolecular bond D, Eq. (1), is softened by a factor of 100. All the simulations reported in this paper have also been performed for a $(\psi_2)_{2869}$ cluster [33]; however, all results are qualitatively and even quantitatively similar to those of the $(N_2)_{2869}$ cluster and will not be reported here. However, the internal excitation of fragmented molecules is drastically affected by the vibrational excitation and is discussed here. For free ψ_2 molecules, we determine the vibrational energy as the sum of the internal kinetic energy of motion parallel to the molecule axis and the intramolecular potential energy, Eq. (1).

Figure 8 shows the internal excitation of these molecules. Again, as in Fig. 7(a), only the molecules in the lateral jet—i.e., with emission angles $\vartheta > 85°$—are displayed. We observe that the *total* internal excitation is comparable to that of the N_2 molecules. However, vibrational excitation dominates over rotational excitation. This vibrational excitation is a feature which these molecules have retained from their formation process, where during the cluster-surface impact, ψ_2 molecules have been strongly vibrationally excited.

However, rotational and vibrational excitations attain similar values. At the highest impact energy studied, for in-

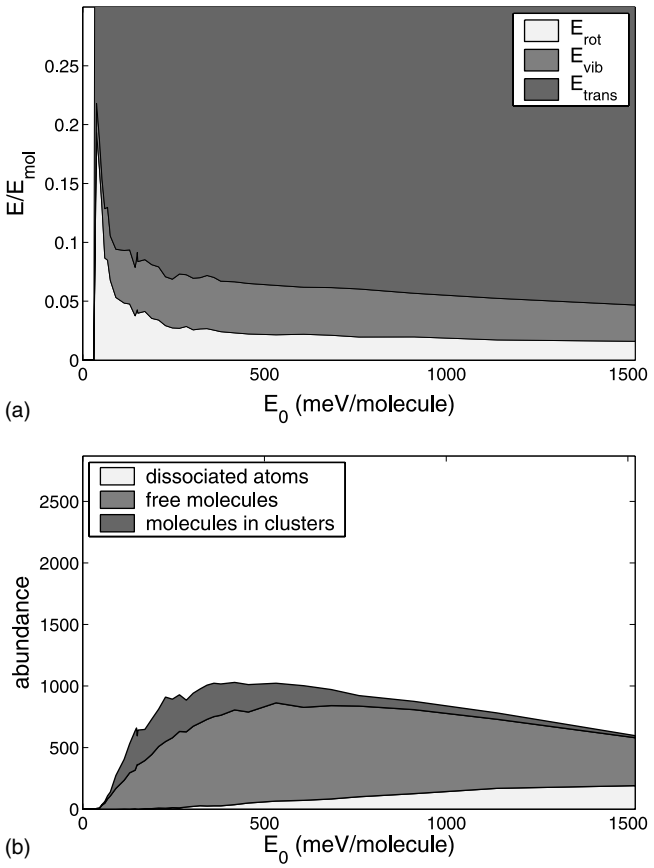

FIG. 8. Analogous to Fig. 7, but for model molecules ψ_2. Here, also vibrational excitation and molecule dissociation have been included.

stance, the ratio $E_{\mathrm{rot}}:E_{\mathrm{vib}}:E_{\mathrm{trans}}=0.015:0.031:0.954$. Thus the total internal molecular energy is only 5% of the translational energy, less than in the case of the N_2 cluster studied above. The internal degrees of freedom are not in thermal equilibrium, which would require that the two rotational degrees of freedom attain the same energy as the vibrational degree of freedom. Rather, vibration is excited with double the energy of rotations.

From our consideration of the molecule excitations shown in Figs. 7(a) and 8(a), we hence conclude that the translational and internal degrees of freedom of the molecules are not in thermal equilibrium. This can be understood from the molecule formation process in the hot, dense collision zone at the surface. Thus our findings show that the concept of a *temperature*, implying thermal equilibration among the atoms or molecules and, in particular, between their different degrees of freedom, must be used with care. This applies in particular to the concept of *thermal femtosecond chemistry*, as introduced by Schek *et al.* [17], but also to statistical approaches such as that by Raz *et al.* [15], who employ concepts such as the *temperature after impact*.

In analogy to Fig. 7(b), Fig. 8(b) shows the contribution of clusters, free molecules, and dissociated atoms to the lateral jets. Now clusters are seen to survive for higher energies: This is due to the fact that now vibrational excitation of cluster fragments offers a new energy channel, which lets them (metastably) better survive the excitation process. On the other hand, molecules may dissociate into atoms; the atomic fraction increases more or less linearly with impact energy.

Interestingly, the jet now has its maximum at a slightly smaller impact energy, $E_0=200$ meV/molecule, than that of N_2 molecules, Fig. 7(b), and—more importantly—the number of molecules in the lateral jet decreases more strongly with impact energy. These features point at the important role of vibrational excitation in the cluster-surface interaction event.

Thus the comparison of Figs. 7 and 8 demonstrates how the intramolecular bonding affects the characteristics of the free molecules emitted. Conversely, free molecules may thus be used to give information about their formation process. Due to the nonequilibrium nature of the energy redistribution in these molecules, it may not be easy to calculate these internal excitations using fluid-dynamics approaches.

IV. CONCLUSIONS

As an exemplary case study, we investigate the reflection of an $(N_2)_{2869}$ cluster off a rigid wall. The technique of molecular-dynamics simulation employed allows us to discuss both the coupling of the translational and internal molecular degrees of freedom and the nonequilibrium fragmentation process of the impacting cluster. We find the following.

(i) Above a threshold energy of roughly $E_{\mathrm{th}}^{\mathrm{frag}}=30$ meV/molecule, the cluster fragments. The number of fragments increases steadily with impact energy, until at around 1100 meV/molecule the cluster has shattered into its molecular constituents. The onset of fragmentation is remarkably similar to that found for an $(N_2)_{13}$ cluster; the energy dependence of the fragmentation process proceeds somewhat smaller than for the small cluster.

(ii) At the fragmentation threshold, almost all the cluster impact energy is converted to internal cluster excitation energy and almost no translational energy remains. With increasing impact energy, the translational energy of the fragments grows considerably more strongly than the internal energy of the fragments.

(iii) As a result, the emerging free molecules possess up to around 95% of the translational energy; this clearly demonstrates the nonequilibrium nature of the monomer formation process.

(iv) In a small energy interval above the fragmentation threshold, the angular distribution changes from a broad backward-directed distribution of "reflected" fragments to a "lateral jetting" distribution, in which the fragments are accelerated away from the point of impact in directions along the surface plane. The latter phenomenon has not been observed for $(N_2)_{13}$ impacts. It is, however, typically observed in fluid-dynamics simulations of liquid droplet impacts and thus demonstrates the close resemblance of the physical mechanisms involved. In fact, in fluid-dynamic calculations this jetting phenomenon shows up independently of the cluster size. The reason hereto is the lack of an intrinsic length scale in these simulations with which to compare the cluster diameter. In molecular-dynamics simulations, on the other

hand, the interatomic distance provides such an intrinsic length scale, and hence the jetting phenomenon becomes dependent of the cluster size.

(v) Due to their intramolecular stiffness, N_2 clusters are not vibrationally excited at the impact energies considered here. We investigated the importance of vibrational excitation by arbitrarily weakening the intramolecular bond strength. The impact of a cluster consisting of these model molecules ψ_2 gives in many respects the same results as for true N_2: fragmentation pattern, onset of lateral jetting. In addition, naturally, the dissociation of molecules is observed. The most drastic difference to N_2 impact is, however, in the energy distribution of the emerging free molecules. In these, rotational excitation is suppressed to the favor of vibrational excitation. This feature demonstrates the strong vibrational excitation occurring during the cluster-surface interaction process which is then conserved in the lateral jets. From this comparison of N_2 and ψ_2 clusters, it must be concluded that the details of the intramolecular bonding play an important role in the cluster-surface collision process and, hence, also in the characteristics of the desorbed molecular fragments.

ACKNOWLEDGMENTS

We acknowledge the Regionales Hochschulrechenzentrum Kaiserslautern for making available their computing resources.

[1] W. Harbich, in *Metal Clusters at Surfaces: Structure, Quantum Properties, Physical Chemistry*, Springer Series in Cluster Physics (Springer, Berlin, 2000), p. 107.
[2] H.-P. Cheng and U. Landman, Science **260**, 1304 (1993).
[3] I. Yamada, J. Matsuo, Z. Insepov, T. Aoki, T. Seki, and N. Toyoda, Nucl. Instrum. Methods Phys. Res. B **164–165**, 944 (2000).
[4] W. Christen and U. Even, J. Phys. Chem. A **102**, 9420 (1998).
[5] C. L. Cleveland and U. Landman, Science **257**, 355 (1992).
[6] B. Gergen, H. Nienhaus, W. H. Weinberg, and E. W. McFarland, Science **294**, 2521 (2001).
[7] K. K. Haller, Y. Ventikos, D. Poulikakosa, and P. Monkewitz, J. Appl. Phys. **92**, 2821 (2002).
[8] C. T. Reimann, Mat. Fys. Medd. K. Dan. Vidensk. Selsk. **43**, 351 (1993).
[9] A. Tomsic, P. U. Andersson, N. Markovic, and J. B. C. Pettersson, J. Chem. Phys. **119**, 4916 (2003).
[10] A. Tomsic, H. Schröder, K.-L. Kompa, and C. R. Gebhardt, J. Chem. Phys. **119**, 6314 (2003).
[11] W. Christen, U. Even, T. Raz, and R. D. Levine, J. Chem. Phys. **108**, 10262 (1998).
[12] G.-Q. Xu, S. L. Bernasek, and J. C. Tully, J. Chem. Phys. **88**, 3376 (1988).
[13] J. N. Beauregard and H. R. Mayne, J. Chem. Phys. **99**, 6667 (1993).
[14] E. Hendell, U. Even, T. Raz, and R. D. Levine, Phys. Rev. Lett. **75**, 2670 (1995).
[15] T. Raz, U. Even, and R. D. Levine, J. Chem. Phys. **103**, 5394 (1995).
[16] W. Christen, U. Even, T. Raz, and R. D. Levine, Int. J. Mass Spectrom. Ion Process. **174**, 35 (1998).
[17] I. Schek, T. Raz, R. D. Levine, and J. Jortner, J. Chem. Phys. **101**, 8596 (1994).
[18] W. Christen and U. Even, Eur. Phys. J. D **9**, 29 (1999).
[19] T. Raz and R. D. Levine, J. Chem. Phys. **105**, 8097 (1996).
[20] S. Zimmermann and H. M. Urbassek, Eur. Phys. J. D **39**, 423 (2006).
[21] A. L. Mackay, Acta Crystallogr. **15**, 916 (1962).
[22] T. P. Martin, Phys. Rep. **273**, 199 (1996).
[23] The icosahedral cluster was constructed using the algorithm by Y. Wang, http://www.pas.rochester.edu/wangyt/algorithms/ih/index.html
[24] D. J. Wales and J. P. K. Doye, J. Phys. Chem. A **101**, 5111 (1997).
[25] Y. Wang, S. Teitel, and C. Dellago, J. Phys. Chem. **122**, 214722 (2005).
[26] G. Herzberg, *Molecular Spectra and Molecular Structure* (Van Nostrand, Toronto, 1950), vol. 1.
[27] A. Lofthus and P. H. Krupenie, J. Phys. Chem. Ref. Data **6**, 113 (1977).
[28] T. A. Scott, Phys. Rep. **27**, 89 (1976).
[29] C. S. Murthy, K. Singer, M. I. Klein, and I. R. McDonald, Mol. Phys. **41**, 1387 (1980).
[30] H. Gades and H. M. Urbassek, Phys. Rev. B **51**, 14559 (1995).
[31] S. D. Stoddard, J. Comput. Phys. **27**, 291 (1978).
[32] R. D. Levine and R. B. Bernstein, *Molecular Reaction Dynamics and Chemical Reactivity* (Oxford University Press, Oxford, 1987).
[33] S. Zimmermann, Ph.D. thesis, University Kaiserslautern, 2006.